Journal of Sustainable Metallurgy
https://doi.org/10.1007/s40831-024-00923-1

RESEARCH ARTICLE

Promoting the Utilization of High-Alumina Iron Ores During Sintering by Pre-preparing a Low-Melting-Point Flux

Junjie Zeng[1,2] · Jin Wang[1,2] · Rui Wang[1,2] · Ningyu Zhang[1,2] · Yongda Li[1,2] · Yuxiao Xue[1,2] · Xuewei Lv[1,2]

Received: 19 May 2024 / Accepted: 27 August 2024

Abstract

High-alumina iron ore sintering is characterized by poor sinter indices and high carbon emission due to the limited formation amount of liquid phase. In this study, the conventional Ca-bearing flux (i.e., burnt lime) was substituted by a new Ca-bearing flux with low melting point (i.e., prefabricated calcium ferrite) for the improvement of the formation ability of liquid phase during sintering. The substitution of prefabricated calcium ferrite for burnt lime contributed to the reduction of the formation temperature of liquid phase and the improvement of liquid-phase fluidity. At the optimum substitution ratio of 20%, the strength of sinter compacts was improved by 38.38% in the mini-sintering tests due to the more formation of liquid phase, especially SFCA (i.e., Silico-ferrite of calcium and alumina). In addition, the proportion of high-alumina iron ore can be appropriately increased from 10.20% to 25.20% at the substitution ratio of 20% under the premise of the similar strength of sinter compacts. High-alumina iron ore can be effectively utilized during sintering by pre-preparing the low melting-point flux, which will be further proved by the relevant sinter pot tests in our follow-up study.

Graphical Abstract

SR(0%~40%): Microstructure of sinter compacts at different substitution ratios of flux A under optical microscope
SR(10.2%~30.2%): Microstructure of sinter compacts at different ratios of high-alumina iron ore D under optical microscope

SR: Substitution ratio of flux A
DR: Iron ore D ratio
M: Magnetite
H: Hematite
F: Fayalite phase
SFCA: Silico-ferrite of calcium and alumina
P: Pore

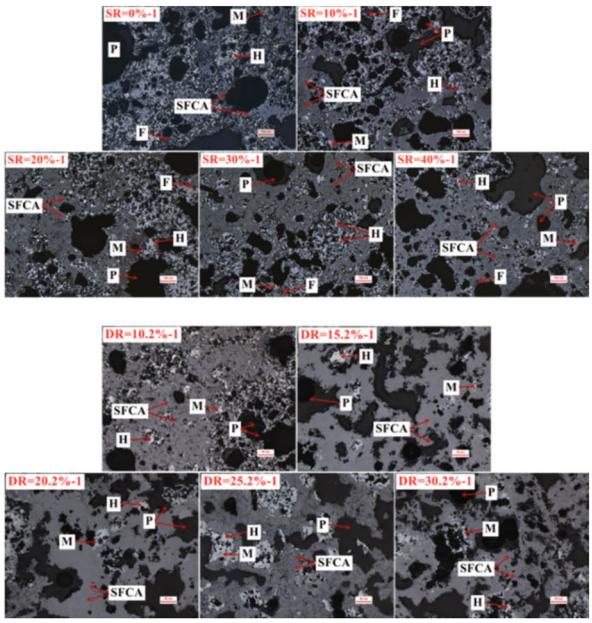

Keywords Sintering · High-alumina iron ore · Prefabricated calcium ferrate · Liquid phase

The contributing editor for this article was Nawshad Haque.

Extended author information available on the last page of the article

Published online: 09 September 2024

Introduction

The iron and steel production in China is still dominated by the long process of blast furnace–converter route [1]. Iron ore sinter is the major burden for blast furnace, and its average proportion in blast furnace is generally over 70% [2]. However, the carbon emission of sintering process is huge, which is only next to that of ironmaking process [3]. In addition, the quality of iron ore resources is increasing deteriorated with the large consumption of high-grade iron ore resources. The proportion of low-grade iron ore resources is increasing, especially high-alumina iron ore [4–6]. Its high Al_2O_3 content leads to the increase of the formation temperature and viscosity of liquid phase during sintering [7–9]. Higher consumption of solid fuel is needed for the adequate formation amount of liquid phase [10, 11], which not only leads to the deterioration of the technical and economic indices of product sinter [9], but also results in the further increase of carbon emission in sintering process [12–14]. In the conventional sintering process, the solid fuel consumption of high-alumina iron ore sintering reaches 70–90 kg/t, which is much higher than that of ordinary iron ore sintering (30–50 kg/t). Promoting the formation of liquid phase is key for the low-carbon sintering of high-alumina iron ore.

At present, numerous studies on the low-carbon sintering technology of iron ores have been conducted mainly including matching optimization sintering technology [15, 16], strengthening granulation technology [17], deep-bed sintering technology [18], flue gas circulation sintering technology [19, 20], and biomass fuel sintering technology [21]. However, there are still some limitations in the application of these techniques for high-alumina iron ore sintering. Matching optimization sintering technology is mainly based on the complementary principle of normal and high-temperature characteristics of iron ores. However, the proportion of high-alumina iron ore is severely limited (generally $\leq 50\%$) due to the excessive variations in the types and compositions of the iron ores. The reduction of carbon emissions is achieved in deep-bed sintering process by improving the self-heat storage of sinter bed and prolonging the holding time of high-temperature zone. The permeability of sinter bed is gradually deteriorated with the increase of its height. In general, the height of sinter bed is not exceeding 1000 mm, which is a great limitation for carbon emission reduction. Carbon emission can be reduced in flue gas circulation sintering process by the improvement of sintering heating conditions, while the result is not very ideal due to the low percentage of flue gas recirculation (20–50%), insufficient O_2 content (10–15%), and high humidity (> 10%) [22]. In addition, strengthening granulation technology mainly aims to the improvement of the permeability of sinter bed, and the pretreatment process of raw materials is always needed. In biomass fuel sintering technology, the fossil fuels such as coke are substituted by the clean biomass fuels for carbon emission reduction [23, 24]. However, the substitution ratio of biomass fuels is generally not exceeding 40% due to the excellent reactivity and fast combustion rate.

During high-alumina iron ore sintering, liquid phases are very difficult to be formed due to it high Al_2O_3 content and poor reactivity of Al-bearing minerals, which is the major reason for its poor sinter indices and high carbon emission. In sintering process, calcium ferrite is the optimal type of liquid phase with low melting point, strong bonding ability, and fluidity reducibility [25, 26]. If calcium ferrate is pre-prepared as a substitute for the conventional Ca-bearing fluxes such as burnt lime, the formation ability of liquid phase would be improved with the reduction of formation temperature of liquid phase. Currently, calcium ferrite is mainly used in iron ore sintering for the treatment of NO_x [27]. The relevant studies are rarely conducted on the promotion of liquid-phase formation. In addition, the action mechanism of the flux of calcium ferrite is still unclear.

In this paper, based on the characterization of the prefabricated calcium ferrite, mini-sintering tests were conducted with the optimization of the substitution of prefabricated calcium ferrite for burnt lime and the proportion of high-alumina iron ore. The action mechanism was revealed by the analyses of the formation temperature and fluidity of liquid phase and the mineralogy of sinter compacts.

Materials and Methods

Raw Materials

The used raw materials mainly include six types of iron ores (A–F), limestone, burnt lime, and a low-melting flux A, which are all provided by a steel plant in China. The chemical compositions of the raw materials are shown in Table 1. Iron ores B, C, and D contain relatively higher contents of Al_2O_3, especially iron ore D. Limestone and burnt lime are both the conventional fluxes for sintering. Flux A was pre-prepared via the rotary kiln process by using the ordinary iron ores, limestone, and burnt lime. Combined with Table 1 and Fig. 1, flux A is mainly in form of $2CaO–Fe_2O_3$ and $CaO–Fe_2O_3$, which is consequently defined as the prefabricated calcium ferrate. It contains 36.47% TFe and 26.12% CaO, and its melting temperature is as low as 1224 °C as shown in Fig. 2. Thus, flux A can be used as a low-melting-point flux for sintering. In addition, the size distributions of all raw materials are kept at − 0.074 mm during mini-sintering tests.

Table 1 Chemical compositions of raw materials (mass-%)

Types	TFe	CaO	SiO_2	MgO	Al_2O_3	P	K_2O	Na_2O	LOI
Iron ore A	62.60	0.19	7.60	0.10	1.50	0.083	0.010	0.010	1.80
Iron ore B	56.50	0.01	6.00	0.10	2.80	0.100	0.010	0.010	9.00
Iron ore C	60.00	0.19	4.30	0.10	3.00	0.120	0.006	0.010	6.00
Iron ore D	55.00	0.15	8.00	0.10	6.50	0.078	0.020	0.080	6.00
Iron ore E	66.80	0.20	5.50	0.60	0.60	0.005	0.043	0.059	− 2.20
Iron ore F	65.30	0.55	7.50	0.10	1.02	0.005	0.043	0.059	− 2.20
Limestone	–	52.50	1.90	1.80	0.18	0.010	–	–	42.00
Flux A	36.47	26.12	1.11	0.12	0.14	0.008	–	–	6.20
Burnt lime	–	85.00	3.00	1.00	0.47	0.010	–	–	0.00

TFe total Fe content, *LOI* loss on ignition

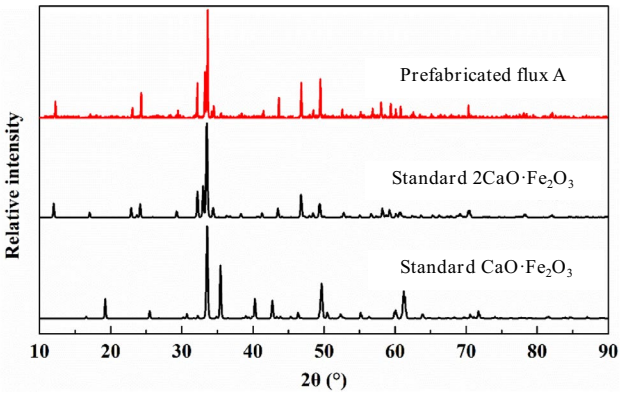

Fig. 1 X-ray diffractions (XRD) of flux A

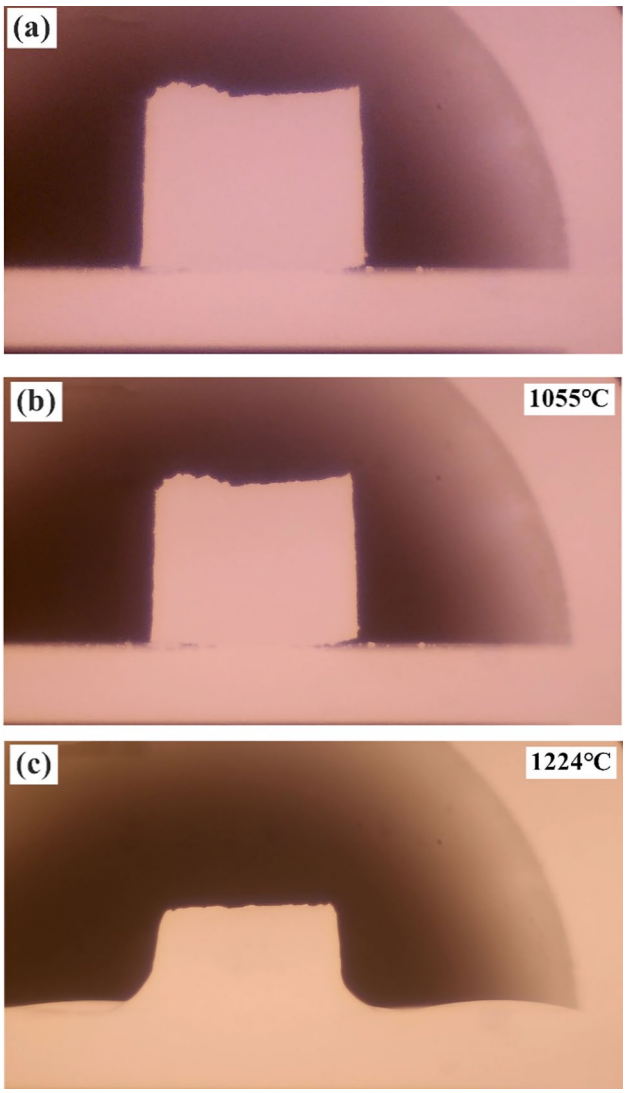

Fig. 2 Melting characteristics of flux A **a** initial state, **b** softening temperature, **c** melting temperature

Experimental Procedure

Mini-Sintering Tests

In mini-sintering tests, the basicity (i.e., the mass ratio of CaO/SiO_2) of sinter compacts was kept at 2.0. The substitution ratio of flux A for burnt lime was optimized from 0 to 40%. The blending of raw materials at different substitution ratio of flux A is listed in Table 2. The substitution ratio was defined as shown in Eq. 1. At the appropriate substitution ratio, the proportion of high-alumina iron ore D was adjusted from the base case (10.20%) to 30.20%. The blending of raw materials at different ratio of iron D is listed in Table 3. The theoretical composition of compacts is shown in Table 4. The detailed method was presented as follows.

First, the raw materials were blended uniformly in the designed proportions and then compacted into ore compacts with 12 mm in diameter and 10 mm in height at the fixed pressure of 3 kN for 1 min. Subsequently, eight ore compacts were put into a porcelain boat with 25 mL in volume. When the sintering temperature reached 1300 °C, the boat was loaded into a horizontal tube furnace with 600 mm in diameter and 1000 mm in length and moved to the target zone in 5 min.

Table 2 The blending of raw materials at different substitution ratios of flux A (mass-%)

Substitution ratio of flux A	Iron A	Iron B	Iron C	Iron D	Iron E	Iron F	Limestone	Burnt lime	Flux A
0	7.15	28.58	21.44	8.57	11.15	7.15	8.88	7.10	0.00
10	7.03	28.14	21.10	8.44	10.97	7.03	8.19	6.55	2.53
20	6.91	27.65	20.74	8.30	10.78	6.91	7.50	6.00	5.20
30	6.79	27.14	20.36	8.14	10.59	6.79	6.75	5.40	8.05
40	6.66	26.64	19.98	7.99	10.39	6.66	5.94	4.75	11.00

Table 3 The blending of raw materials at different ratios of iron D (mass-%)

Ratio of iron D	Iron A	Iron B	Iron C	Iron D	Iron E	Iron F	Limestone	Burnt lime	Flux A
10.20	6.91	27.65	20.74	8.29	10.79	6.91	7.50	6.00	5.20
15.20	6.88	27.51	16.59	12.29	10.73	6.88	7.66	6.13	5.32
20.20	6.83	27.33	12.46	16.23	10.66	6.83	7.88	6.30	5.47
25.20	6.79	27.17	8.40	20.13	10.60	6.79	8.06	6.45	5.60
30.20	6.75	27.01	4.38	23.98	10.54	6.75	8.25	6.60	5.73

Table 4 The theoretical compositions of compacts (mass-%)

Types		TFe	CaO	SiO_2	MgO	Al_2O_3
Substitution ratio of flux A	0	72.70	15.65	7.80	0.54	3.32
	10	73.08	15.44	7.70	0.51	3.28
	20	73.41	15.28	7.59	0.49	3.23
	30	73.80	15.08	7.48	0.46	3.18
	40	74.26	14.81	7.37	0.43	3.13
Ratio of iron D	10.2	73.41	15.28	7.59	0.49	3.23
	15.2	72.73	15.58	7.78	0.49	3.41
	20.2	71.96	15.99	7.95	0.50	3.59
	25.2	71.26	16.34	8.13	0.51	3.77
	30.2	70.55	16.69	8.30	0.51	3.95

After sintered for 5 min, the boat was removed from the furnace at the same speed and cooled to the room temperature in air atmosphere. The compressive strength of sinter compacts was determined by means of a domestic mechanical press, and the average values were obtained. The mineralogy of sinter compacts was analyzed by means of the optical microscope (DM4P, Leica Microsystems, Germany) and scanning electron microscopy and energy-dispersive spectrum (SEM–EDS, Sigma 300, ZEISS, Germany).

$$\text{Substitution ratio} = 0.261W_{\text{Flux A}}/(0.850W_{\text{Burnt lime}} + 0.261W_{\text{Flux A}}) \times 100\%, \quad (1)$$

where: $W_{\text{Flux A}}$: Mass of flux A, kg; $W_{Burnt\ lime}$: Mass of burnt lime, kg; 0.261: Mass ratio of CaO in flux A; 0.850: Mass ratio of CaO in burnt lime.

Determination of Melting Characteristics and Liquid-Phase Fluidity

The melting characteristics of flux A were determined in a high-temperature horizontal tube furnace (Φ 14 × 280 mm) equipped with a high-resolution digital camera as shown in Fig. 3. First, the sample of flux A was compacted into a cylinder with 3 mm in diameter and 5 mm in height. Subsequently, the cylinder was placed on a square corundum substrate with 15 mm in length, 10 mm in width, and 3 mm in thickness. After the substrate was loaded into the

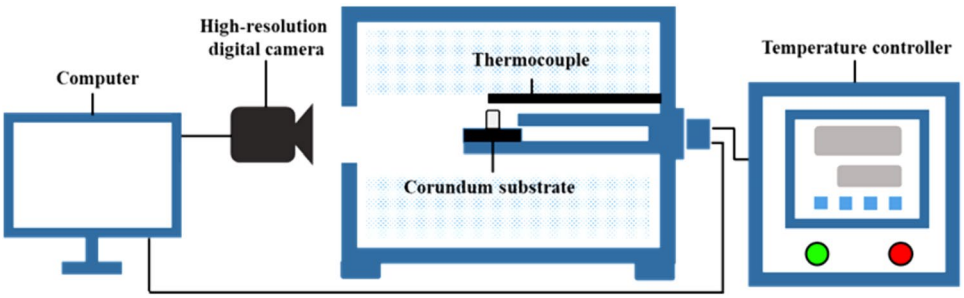

Fig. 3 Equipment diagram of melting characteristics and liquid-phase fluidity

horizontal tube furnace, the heating program was started with a heating rate of 5 °C/min. The sample was gradually melted in air atmosphere. The melting process was recorded by the high-resolution digital camera, and the photos were captured at a rate of 1 frame per second. Initial melting temperature and melting temperature were determined based on the reduction of the sample height in the photos to 1/4 and 2/4 of its initial value, respectively. In addition, the blended ores at different substitution ratio of flux A were prepared according to the methods in "Mini-Sintering tests" section. Its melting characteristics were determined via the same method above for promulgating the effect of flux A on the formation of liquid phase during sintering.

For the characterization of liquid-phase fluidity during sintering, the basicity of the blended ores was increased to 4.0. Similarly, the blended ores were compacted into a cylinder and put on a square corundum substrate with the same size. They are sintered at 1300 °C for 5 min in the horizontal tube furnace under air atmosphere. The sample was cooled to 900 °C in the furnace at a rate of 10 °C/min and then removed from the furnace and further cooled to the room temperature under air atmosphere. The liquid-phase fluidity index was determined according to the Eq. (2) [28].

$$LI = S_1/S_0 - 1, \tag{2}$$

where LI: liquid-phase fluidity index; S_1: area of the sintered compact; and S_0: area of the initial compact.

Results

Influence of the Substitution Ratio of Flux A for Burnt Lime

The variation of the strength of sinter compacts with the substitution ratio of flux A is shown in Fig. 4. As the substitution ratio of flux A is increased from 0 to 30%, the strength of sinter compacts is increased significantly from 24.88 MPa to 36.92 MPa. When the substitution ratio of flux A is further increased to 40%, the strength of sinter compacts is decreased to 34.63 MPa. It can be observed

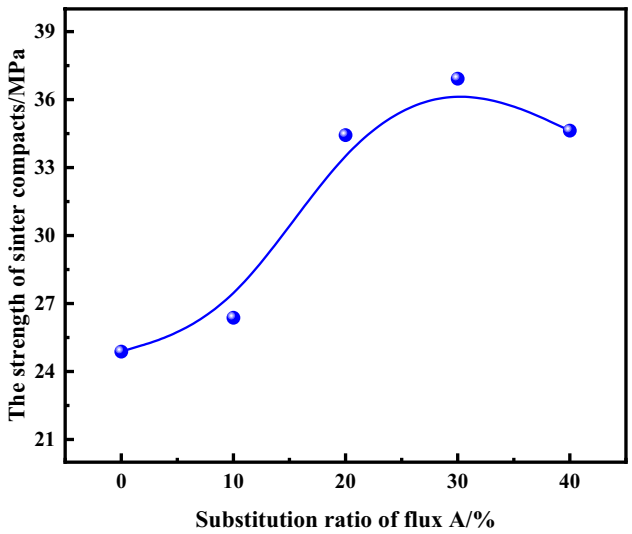

Fig. 4 Influence of the substitution ratio of flux A on the strength of sinter compacts

that the increased extent of the strength of sinter compacts is much higher with the substitution ratio of flux A increased to 20%. Under this condition, the strength of sinter compacts is greatly improved by 38.38% compared with the base case. Thus, the appropriate substitution ratio of flux A should be 20% in the comprehensive consideration of the strength of sinter compacts and preparation costs of flux A.

Influence of High-Alumina Iron Ore D Ratio

The variation of the strength of sinter compacts with the ratio of high-alumina iron ore D is shown in Fig. 5, when the substitution ratio of flux A for burnt lime is kept at 20%. When the ratio of high-alumina iron ore D is increased from 10.20% to 25.20%, the strength of sinter compacts remains stable, which is slightly reduced from 34.43 MPa to 33.82 MPa. With the further increase of the ratio of high-alumina iron ore D to 30.20%, the strength of sinter compacts is obviously reduced to 32.44 MPa. At the substitution ratio of flux A of 20%, the ratio of high-alumina iron ore D can be increased by 15.00% under the premise of the equal strength of sinter compacts. The results indicates

that the substitution of flux A for burnt lime contributes to the more effective utilization of high-alumina iron ore D during sintering.

Discussion

Melting Characteristics of Blended Ores

The variations of the melting characteristics of blended ores with the substitution ratio of flux A for burnt lime are shown in Fig. 6. As the substitution ratio of flux A is increased from 0 to 40%, the softening temperature and hemisphere temperature are obviously reduced from 1285 °C and 1410 °C to 1247 °C and 1355 °C, respectively. The results indicate that the increase of the substitution ratio of flux A contributes to the reduction of the formation temperature of liquid phase during sintering. Thus, less solid fuel consumption and better sinter indices can be achieved due to the improvement of the formation ability of liquid phase.

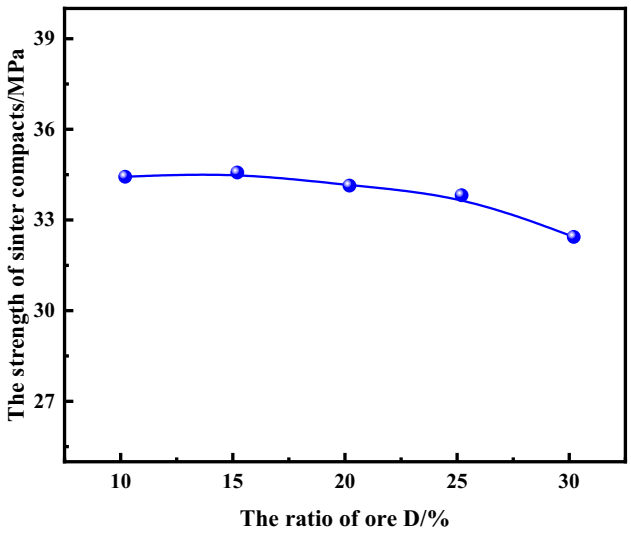

Fig. 5 Influence of high-alumina iron ore D on the strength of sinter compacts

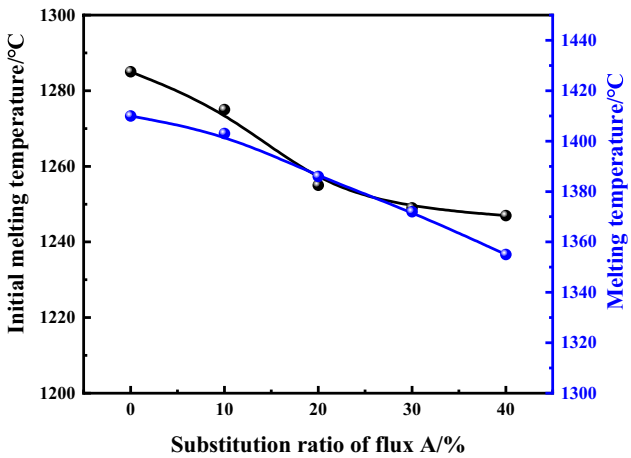

Fig. 6 Variations of melting characteristic temperatures with the substitution ratio of flux A

Fluidity of Liquid Phase During Sintering

The variations of the fluidity of liquid phase of blended ores with the substitution ratio of flux A for burnt lime are shown in Fig. 7. As the substitution ratio of flux A is increased from 0 to 30%, the liquid-phase fluidity index is greatly increased from 12.4 to 20.74. When the substitution ratio of flux A is further increased to 40%, the liquid-phase flow index is further increased to 21.27. The results indicate that the partial substitution of flux A contributes to fluidity of liquid phase during sintering, which is conducive to the improvement of the solid–liquid bonding effect and the strength of sintered compacts. Consequently, less solid fuel consumption and better sinter indices can be achieved. However, the overhigh liquid-phase fluidity is adverse to sintering process due to the excessive extending of liquid phase and the more formation of large pores.

Mineralogy of Sinter Compacts

Action of Low Melting-Point Flux A

The microstructure of sinter compacts at different substitution ratios of flux A) is shown in Figs. 8 and

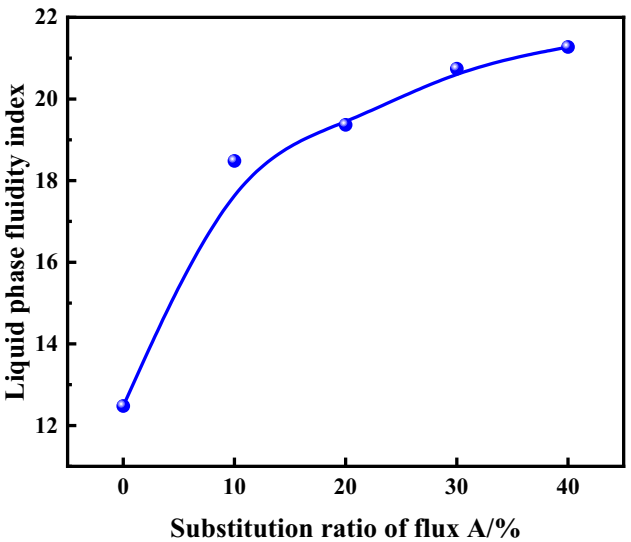

Fig. 7 Effect of the substitution ratio of flux A on the fluidity of liquid phase during sintering

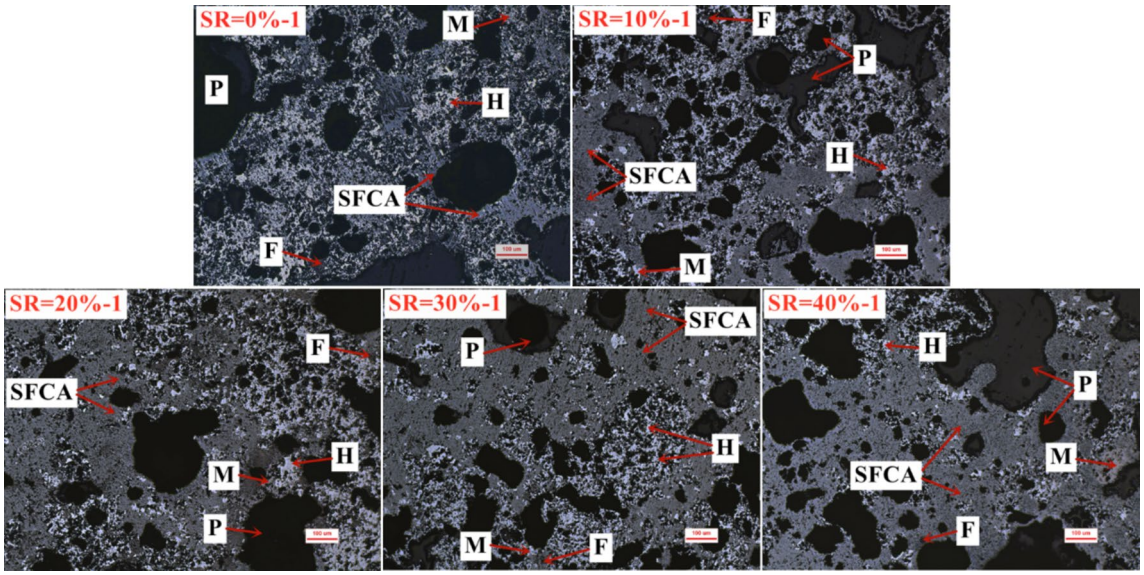

Fig. 8 Microstructure of sinter compacts at different substitution ratios of flux A under optical microscope. *SR* substitution ratio of flux A, *M* magnetite, *H* hematite, *F* fayalite phase, *SFCA* silico-ferrite of calcium and alumina, *P* pore

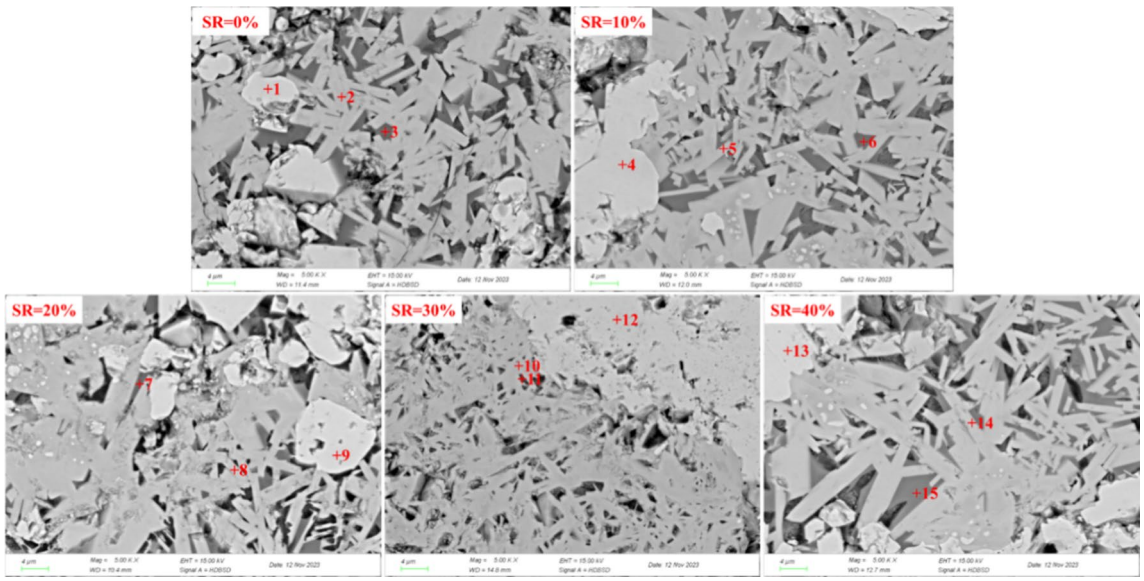

Fig. 9 Microstructure of sinter compacts at different substitution ratios of flux A under SEM. *SR* Substitution ratio of flux A

9. Combined with Table 5 and Fig. 10, sinter compacts in the base case possess large pores with thin wall and the porosity is as high as 43.03% while SFCA amount is limited (i.e., 22.87%). With the substitution ratio of flux A increased to 20%, the porosity of sinter compacts is reduced to 28.98% and the connectivity of pores is also weakened. Meanwhile, SFCA amount is increased to 76.29% due to the reduction of the formation temperature of liquid phase and the improvement of liquid-phase fluidity. When the substitution ratio of flux A is further increased to 40%, SFCA is continuously increased to 91.54%. However, the pores are increasingly irregular and the porosity is also increased to 49.53%, which is mainly due to the excessive expansion of liquid phase. Overall, the substitution of flux A for burnt lime contributes to the formation of liquid phase, especially SFCA. However, the overhigh amount of liquid phase is adverse to the consolidation of sinter compacts. Thus, the recommended substitution ratio of flux A is 20% which is consistent

Table 5 EDS analysis of the marked points in Fig. 9

Point No	Elemental compositions/(mass-%)						Phases
	Fe	Ca	Si	Al	Mg	O	
1	72.42	0.34	0.00	0.41	0.00	26.83	Hematite
2	56.08	9.94	2.56	2.07	0.31	29.05	SFCA
3	15.74	28.16	15.64	1.24	0.11	39.10	Fayalite
4	72.36	0.21	0.04	0.43	0.00	26.96	Hematite
5	53.08	10.39	3.28	2.17	0.35	30.73	SFCA
6	15.62	27.26	16.22	1.87	0.17	38.87	Fayalite
7	19.03	24.78	14.02	2.63	0.35	39.20	Fayalite
8	45.61	14.91	4.90	1.65	0.40	32.52	SFCA
9	72.10	0.35	0.00	0.55	0.03	26.97	Hematite
10	54.92	9.79	2.33	1.65	0.22	31.07	SFCA
11	37.01	23.68	8.67	0.96	0.13	29.55	Fayalite
12	70.82	0.11	0.10	0.09	0.00	28.88	Hematite
13	71.92	0.30	0.01	0.05	0.00	27.72	Hematite
14	42.50	14.94	7.70	1.61	0.22	33.02	SFCA
15	19.33	24.28	15.49	1.62	0.23	39.05	Fayalite

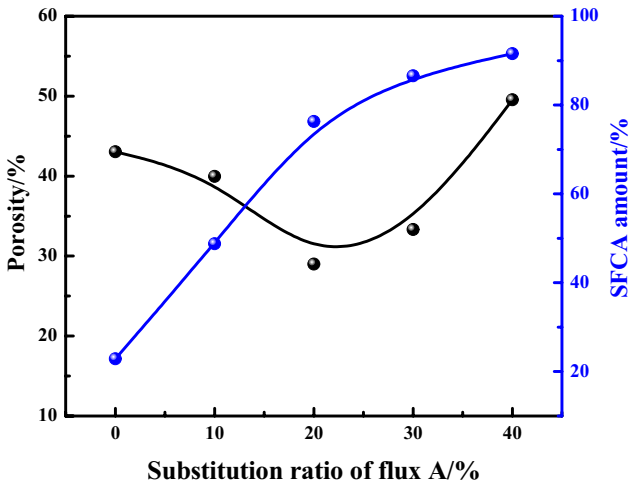

Fig. 10 Porosity and SFCA amount of sinter compacts at different substitution ratios of flux A

with the results in "Influence of the substitution ratio of flux A for burnt lime" section.

Increase of High-Alumina Iron Ore D Ratio

The microstructure of sinter compacts at different ratios of high-alumina iron ore D is shown in Figs. 11 and 12 when the substitution ratio of flux A is 20%. With the increase of high-alumina iron ore D ratio from 10.20% to 25.20%, the pore structure in sinter compacts is transformed from approximative circular pores to irregular pores, and the porosity is slightly increased due to the increase of Al_2O_3 content. However, the strength of sinter compacts can still remain stable due to the more formation of SFCA combined with Table 6. Thus, the strength of sinter compacts can be maintained stable as shown in Fig. 5. When the ratio of high-alumina iron ore D is further increased to 30.20%, pore structure with the greater deformation degree, much larger diameter and higher connectivity is formed and the porosity of sinter compacts is obviously increased. Furthermore, the solid phases such as hematite and magnetite cannot be well wetted by SFCA. The strength of sinter compacts is obviously reduced at the high-alumina iron ore D ratio of 30.20%. Consequently, the ratio of high-alumina iron ore D can be increased by 15.00% when the substitution ratio of flux A for burnt lime is 20%. In the follow-up study, the relevant sinter pot tests would be conducted for the further investigation on the positive effect of the low melting-point flux on the utilization of high-alumina iron ores during sintering.

Conclusion

(1) The prefabricated calcium ferrate (i.e., flux A) contains 36.47% TFe and 26.12% CaO and its melting temperature is as low as 1224 °C, which can be used as a new low melting-point flux for promoting the formation of liquid phase during high-alumina iron ore sintering.

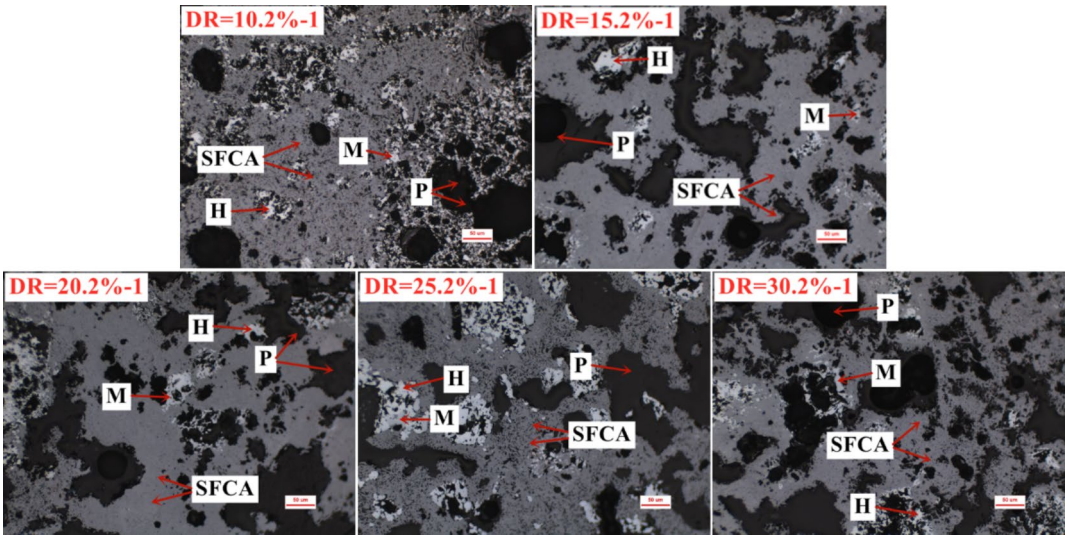

Fig. 11 Microstructure of sinter compacts at different ratios of high-alumina iron ore D under optical microscope. *DR* iron ore D ratio, *M* magnetite, *H* hematite, *F* fayalite phase, *SFCA* silico-ferrite of calcium and alumina, *P* pore

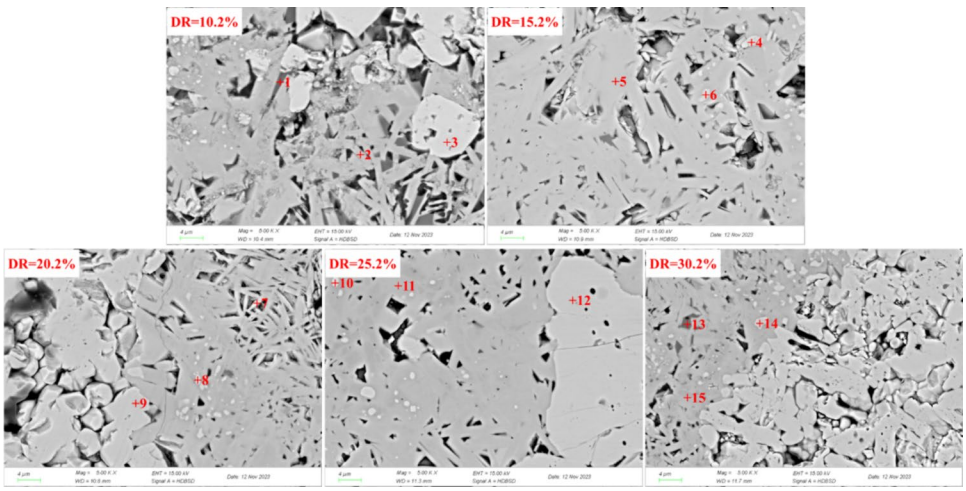

Fig. 12 Microstructure of sinter compacts at different ratios of high-alumina iron ore D under SEM. *DR* iron ore D ratio)

(2) With the optimization of the substitution ratio of flux A for burnt lime, the strength of sinter compacts can be improved by 38.38% compared with the base case when the substitution ratio of flux A is 20%. Based on this, the proportion of high-alumina iron ore can be increased from 10.20% to 25.20% when the strength of sinter compacts is kept stable.

(3) The substitution of flux A for burnt lime contributes to the reduction of the formation temperature of liquid phase and the improvement of liquid-phase fluidity. The high-alumina iron ore can be more effectively utilized in sintering process when the substitution of flux A is 20% due to the improvement of formation ability of liquid phase, especially SFCA. The relevant sinter pot tests would be conducted in the next-step study for the further elucidation of the action mechanism of flux A on high-alumina iron ore sintering.

Table 6 EDS analysis of the marked points in Fig. 12

Point No	Elemental compositions/(mass-%)						Phases
	Fe	Ca	Si	Al	Mg	O	
1	19.03	24.78	14.02	2.63	0.35	39.20	Fayalite
2	45.61	14.91	4.90	1.65	0.40	32.52	SFCA
3	72.10	0.35	0.00	0.55	0.03	26.97	Hematite
4	72.63	0.35	0.00	0.87	0.04	26.10	Hematite
5	51.74	8.21	2.56	7.43	0.10	29.96	SFCA
6	71.08	0.13	0.05	1.91	0.00	26.84	Hematite
7	72.63	0.35	0.00	0.87	0.04	26.10	Hematite
8	51.74	8.21	2.56	7.43	0.10	29.96	SFCA
9	71.08	0.13	0.05	1.91	0.00	26.84	Hematite
10	72.63	0.35	0.00	0.87	0.04	26.10	Hematite
11	51.74	8.21	2.56	7.43	0.10	29.96	SFCA
12	71.08	0.13	0.05	1.91	0.00	26.84	Hematite
13	72.63	0.35	0.00	0.87	0.04	26.10	Hematite
14	51.74	8.21	2.56	7.43	0.10	29.96	SFCA
15	71.08	0.13	0.05	1.91	0.00	26.84	Hematite

Acknowledgements Financial support from Youth National Natural Science Foundation of China (Grant No. 52304344), Fundamental Research Funds for the Central Universities (Grant No. 2023CDJXY-016), and Post-doctoral Innovator Project of Chongqing (Grant No. CQBX202225) are sincerely acknowledged.

Funding This work was funded by Youth National Natural Science Foundation of China, 52304344, Yuxiao Xue, Fundamental Research Funds for the Central Universities, 2023CDJXY-016, Xuewei Lv, Post-doctoral Innovator Project of Chongqing, CQBX202225, Yuxiao Xue.

Declarations

Conflict of interest On behalf of all authors, the corresponding author states that there is no conflict of interest.

References

1. Pownceby MI, Webster NAS, Manuel JR, Ware N (2016) The influence of ore composition on sinter phase mineralogy and strength. Miner Process Extr Metall 125:140–148. https://doi.org/10.1080/03719553.2016.1153276
2. Naito M, Takeda K, Matsui Y (2015) Ironmaking technology for the last 100 years: deployment to advanced technologies from introduction of technological know-how, and evolution to next-generation process. ISIJ Int 55:7–35. https://doi.org/10.2355/isijinternational.55.7
3. Holmes RJ, Lu YF, Lu LM (2022) Introduction: overview of the global iron ore industry. ACS Omega Chapter 1:1–56. https://doi.org/10.1016/b978-0-12-820226-5.00023-9
4. Lu L, Holmes RJ, Manuel JR (2007) Effects of alumina on sintering performance of hematite iron ores. ISIJ Int 04:349–358. https://doi.org/10.2355/isijinternational.47.349
5. Fernández-González D, Ruiz-Bustinza I, Mochón J, González-Gasca C, Verdeja LF (2017) Iron ore sintering: raw materials and granulation. Miner Process Extr Metall Rev 38:36–46. https://doi.org/10.2355/isijinternational1966.28.146
6. Zhang WL, Wang JY, Lin CY (2017) Analysis and countermeasures of using iron ore with high content of Al_2O_3. Metall Eng 04:147–157. https://doi.org/10.1016/b978-1-78242-156-6.00005-8
7. Wu SL, Zhang GL, Chen SL (2014) Influencing factors and effects of assimilation characteristic of iron ores in sintering process. ISIJ Int 54:582–588. https://doi.org/10.2355/isijinternational.54.582
8. Wu SL, Huang W, Kou MY, Liu XL, Du KP, Zhang KF (2015) Influence of Al_2O_3 content on liquid phase proportion and fluidity of primary slag and final slag in blast furnace. Steel Res Int 86:550–556. https://doi.org/10.1002/srin.201400158
9. Xue YX, Pan J, Zhu DQ, Guo ZQ, Tian HY, Shi Y, Lu SH (2021) Effect of alumina occurrence on sintering performance of iron ores and its action mechanism. J Market Res 12:1157–1170. https://doi.org/10.1016/j.jmrt.2021.03.054
10. Machida S, Nushiro K, Ichikawa K, Noda H, Sakai H (2006) Experimental evaluation of chemical composition and viscosity of melts formed during iron ore sintering. Tetsu-to-Hagane 92:755–762. https://doi.org/10.2355/isijinternational.45.513
11. Guo H, Guo XM (2018) Effect of aluminum dissolved in hematite on formation of calcium ferrites at 1473 K. Metall Mater Trans B 49:1974–1984. https://doi.org/10.1007/s11663-018-1292-x
12. Matsumura T, Morioka K, Shimizu M, Noda T, Matsuo T (1996) Mechanism of the non-uniform sintering on using a low-Al_2O_3 pisolite ore. Tetsu-to-Hagané 82:23–28. https://doi.org/10.2355/tetsutohagane1955.82.1-23
13. Sinha M, Ramna RV (2009) Effect of variation of alumina on the microhardness of iron ore sinter phases. ISIJ Int 49:719–721. https://doi.org/10.2355/isijinternational.49.719
14. Loo CE, Leung W (2003) Factors influencing the bonding phase structure of iron ore sinters. ISIJ Int 43:1393–1402. https://doi.org/10.2355/isijinternational.43.1393
15. Gan M, Fan XH, Ji ZY, Chen XL, Yin L, Jiang T, Li GH, Yu ZY (2015) High temperature mineralization behavior of mixtures during iron ore sintering and optimizing methods. ISIJ Int 55:742–750. https://doi.org/10.2355/isijinternational.55.742
16. Wu SL, Zhai XB, Su LX, Ma XD (2020) Ore-blending optimization for Canadian iron concentrate during iron ore sintering based on high-temperature characteristics of fines and

nuclei. J Iron Steel Res Int 27:755–769. https://doi.org/10.1007/s42243-019-00318-7
17. Umadevi T, Deodar AV, Mahapatra PC, Prabhu M, Ranjan M (2009) Influence of alumina on iron ore sinter properties and productivity in the conventional and selective granulation sintering process. Steel Res Int 80:686–692. https://doi.org/10.1002/srin.201000030
18. Han HL, Wu SL, Ma LW, Feng GS, Jiang WZ (2012) Fundamental research on sintering technology with super deep bed achieving energy saving and reduction of emissions. Metall Res Technol 109:249–259. https://doi.org/10.1051/metal/2012028
19. Fan XH, Yu ZY, Gan M, Li WQi, Ji ZY, (2013) Influence of O_2 content in circulating flue gas on iron ore sintering. J Iron Steel Res Int 20:1–6. https://doi.org/10.1016/s1006-706x(13)60103-x
20. Fan XH, Yu ZY, Gan M, Chen XL, Jiang T, Wen HL (2014) Appropriate technology parameters of iron ore sintering process with flue gas recirculation. ISIJ Int 54:2541–2550. https://doi.org/10.2355/isijinternational.54.2541
21. Liu C, Zhang YZ, Zhao K, Xing HW, Kang Y (2019) Effect of biomass on reaction performance of sintering fuel. J Mater Sci 54:3262–3272. https://doi.org/10.1007/s10853-018-3061-2
22. Guang W, Zhang HQ, Su BX, Ma JC, Zuo HB, Wang JS, Xue GQ (2021) The current situation of carbon emission and carbon reduction in Chinese steel industry. Ind Miner Process 50:55–64. https://doi.org/10.1016/j.egypro.2011.03.279
23. Jha G, Soren S, Mehta KD (2020) Life cycle assessment of sintering process for carbon footprint and cost reduction: a comparative study for coke and biomass-derived sintering process. J Clean Prod 259:120889–120913. https://doi.org/10.1016/j.jclepro.2020.120889
24. Gan M, Fan XH, Chen XL, Ji ZY, Lv W, Wang Y, Yu ZY (2012) Reduction of pollutant emission in iron ore sintering process by applying biomass fuels. ISIJ Int 52:1574–1578. https://doi.org/10.2355/isijinternational.52.1574
25. Xue YX, Pan J, Zhu DQ, Guo ZQ, Tian HY (2020) Improving high-alumina iron ores processing via the investigation of the influence of alumina concentration and type on high-temperature characteristics. Minerals 10:802–829. https://doi.org/10.3390/min10090802
26. Li HP, Wu SL, Hong ZB, Zhang WL, Zhou H, Kou MY (2019) The mechanism of the effect of Al_2O_3 content on the liquid phase fluidity of iron ore fines. Processes 7:931. https://doi.org/10.3390/pr7120931
27. Morioka K, Inaba S, Shimizu M, Ano K, Sugiyama T (2000) Primary application of the "in-bed-deNO_x" process using Ca–Fe oxides in iron ore sintering machines. ISIJ Int 40:280–285. https://doi.org/10.2355/isijinternational.40.280
28. Wu SL, Zhang GL, Chen SG, Su B (2014) Influencing factors and effects of assimilation characteristic of iron ores in sintering process. ISIJ Int 54:582–588. https://doi.org/10.2355/isijinternational.54.582

Authors and Affiliations

Junjie Zeng[1,2] · Jin Wang[1,2] · Rui Wang[1,2] · Ningyu Zhang[1,2] · Yongda Li[1,2] · Yuxiao Xue[1,2] · Xuewei Lv[1,2]

✉ Yuxiao Xue
yxxue@cqu.edu.cn

[1] College of Materials Science and Engineering, Chongqing University, Chongqing 400045, PR China

[2] Chongqing Key Laboratory of Vanadium-Titanium Metallurgy and New Materials, Chongqing University, Chongqing 400044, PR China